Environmental Science & Technology

pubs.acs.org/est

Article

Redox Oscillations Activate Thermodynamically Stable Iron Minerals for Enhanced Reactive Oxygen Species Production

Guoqiang Zhao, Mengxi Tan, Binbin Wu, Xiaoshan Zheng, Ruoxuan Xiong, Baoliang Chen, Andreas Kappler, and Chiheng Chu*

Cite This: *Environ. Sci. Technol.* 2023, 57, 8628−8637

Read Online

ACCESS | Metrics & More | Article Recommendations | Supporting Information

ABSTRACT: Reactive oxygen species (ROS) play key roles in driving biogeochemical processes. Recent studies have revealed nonphotochemical electron transfer from redox-active substances (e.g., iron minerals) to oxygen as a new route for ROS production. Yet, naturally occurring iron minerals mainly exist in thermodynamically stable forms, restraining their potential for driving ROS production. Here, we report that tide-induced redox oscillations can activate thermodynamically stable iron minerals for enhanced ROS production. $^{\bullet}OH$ production in intertidal soils (15.8 ± 0.5 $\mu mol/m^2$) was found to be 5.9-fold more efficient than those in supratidal soils. Moreover, incubation of supratidal soils under tidal redox fluctuations dramatically enhanced $^{\bullet}OH$ production by 4.3-fold. The tidal hydrology triggered redox alternation between biotic reduction and abiotic oxidation and could accelerate the production of reactive ferrous ions and amorphous ferric oxyhydroxides, making thermodynamically stable iron minerals into redox-active metastable iron phases (RAMPs) with reduced crystallinity and promoting surface electrochemical activities. Those RAMPs displayed enhanced redox activity for ROS production. Investigations of nationwide coastal soils verified that tide-induced redox oscillations could ubiquitously activate soils for enhanced ROS production. Our study demonstrates the effective formation of RAMPs from redox oscillations by hydrological perturbations, which provides new insights into natural ROS sources.

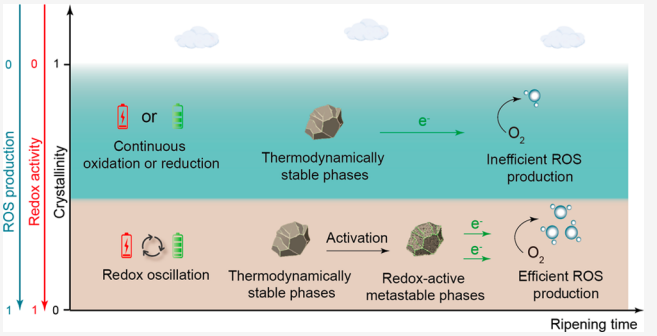

KEYWORDS: *Reactive oxygen species (ROS), Redox oscillation, Hydrological perturbation, Iron minerals, Redox-active metastable phases (RAMPs)*

INTRODUCTION

Reactive oxygen species (ROS) play key roles in the Earth's surface biogeochemical processes and pollutant dynamics.[1] Photochemical processes were historically considered to be the primary drivers of ROS production on the Earth's surface.[2] Recent studies have revealed electron transfer from reduced substances to oxygen as a new route of ROS formation,[2−4] supplementing the classical photochemical path.[5,6] For instance, poorly crystalline iron-bearing minerals exhibit lower thermodynamic stabilities (and higher solubilities[7]) than their corresponding highly crystalline phases with long-range ordering. These poorly crystalline reduced minerals can efficiently activate oxygen to form a series of ROS including hydroxyl radicals ($^{\bullet}OH$), superoxide radicals ($O_2^{\bullet-}$), and hydrogen peroxide (H_2O_2) in the assistance of microbes. Those ROS are suggested to play key roles in mediating carbon cycling[8,9] and pollutant transformation (e.g., cadmium, tetracycline) in soils.[10,11] Nevertheless, iron minerals in natural environments mainly exist as highly crystalline forms,[12,13] which are thermodynamically stable with lower rates and extent of electron acceptance and donation.[14,15] The capability of thermodynamically stable iron minerals for ROS production and potential paths as well as the role of microbes remains largely unknown.

Recent advances suggest that thermodynamically stable iron minerals can be activated under fluctuating redox conditions,[16,17] forming redox-active metastable phases (RAMPs).[12] Iron minerals as RAMPs are intermediate substances (in terms of redox state, structure, crystallinity) before ripening to thermodynamic equilibrium states with higher stability.[12,18] Therefore, iron minerals as RAMPs can act as biogeobatteries by efficiently accepting and donating electrons.[12,19] In aquatic ecosystems, hydrological fluctuations can trigger redox oscillations and activate ripened iron minerals into RAMPs.[12,19,20] The redox-active metastable iron minerals may significantly contribute to biogeochemical processes such as inhibiting methanogenesis from wetlands due to

Received: March 27, 2023
Revised: May 12, 2023
Accepted: May 15, 2023
Published: May 31, 2023

https://doi.org/10.1021/acs.est.3c02302
Environ. Sci. Technol. 2023, 57, 8628−8637

their high electron accepting capacity.[12,21] Yet, a link between iron mineral activation and ROS production is not established.

Coastal wetlands such as intertidal mangroves, mud flats, and salt marshes represent hot spots of fluctuating redox conditions on the Earth's surface[22,23] and are important global carbon[24] and pollutants sinks (e.g., polycyclic aromatic hydrocarbons[25]). The tidal hydrological perturbations induce 1−2 cycles of switching between oxidizing and reducing conditions per day.[22,26] Our recent study has revealed efficient ROS production in coastal soils under tidal conditions.[27] This is surprising given that iron minerals in coastal soils are typically from river-borne clays or marine sediments that are thermodynamically stable.[28] Therefore, we were interested in whether tide-induced fluctuating redox conditions can activate thermodynamically stable iron minerals in coastal soils into RAMPs for enhanced ROS production, which, if the case, will accelerate carbon mineralization and pollutant transformation in coastal ecosystems.

The goal of this study was to investigate the production of RAMPs and ROS from highly crystalline iron minerals under hydrological perturbations. Specifically, we aim to (i) explore enhanced ROS production under tidal conditions, (ii) investigate the redox variation of iron minerals using electrochemical analyses, and (iii) establish a link among tidal hydrology, iron mineral RAMP formations, and ROS production. Further, we examine the generality of tide-activated iron minerals for enhanced ROS production in multiple coastal ecosystems. As a model system to achieve our goal, we chose pyrite and goethite to investigate the redox-cycling activation of iron minerals because they are widely distributed in coastal soils and represent thermodynamically stable iron minerals. Our results help to build a biogeochemical-hydrological framework including the activation of iron minerals under fluctuating redox conditions for enhanced ROS production, which provides new insights into element cycles and pollutant dynamics in regions of frequent hydrological perturbations and redox oscillations.

MATERIALS AND METHODS

Soil Preparation and Tide-Induced Redox Fluctuations. Fresh soils from intertidal wetlands in the Yellow River Delta (119°18′E, 37°48′N) were placed into a custom-made polyethylene pipe (diameter 10 cm), followed by addition of 2 L of oxygen-free seawater containing *Shewanella oneidensis* strain MR-1 (~3.0×10^8 cells/mL). Seawater was prepared by dissolving sea salt (Sigma S9883) into ultrapure water, sterilized by autoclave sterilization, and bubbled with N_2 for 1 h to remove dissolved oxygen. *Shewanella oneidensis* strain MR-1 is a Fe(III)-reducing bacterium widely distributed in marine sediments.[19,29] The soils were sealed with a plastic film and incubated in the dark at room temperature for 14 days. Afterward, the overlying water was drained, and soils were incubated under air for 2 days to finish soil preincubation. We conducted the preincubation to reconstitute microbial activity and establish equilibrium conditions. The tide-induced redox fluctuations were conducted by periodically adding and draining overlying seawater to simulate high tide (12 h) and low tide (12 h), respectively. At designed time points, aliquots (500 μL) were collected from the soil-water interface and immediately mixed with methanol (500 μL), followed by filtration through a 0.22 μm membrane for •OH measurement. Iron minerals in coastal soils partially originate from river clay input. And river-borne clay minerals will undergo tidal activation after they enter intertidal zones. For activation of supratidal soils, river-borne clay minerals collected from the Yellow River in the supratidal zone (119°40′E, 37°47′N) were added to the surface of intertidal soils (thickness 2 cm) in the polyethylene pipes (Figures S1 and S2). The oxygen content at the soil-water interface was measured using a planar optode (thickness 10 μm, dimension= 3 cm × 4 cm) that was summarized in the Supporting Information.

Redox Oscillation Activation of Pyrite and Goethite. To test the ROS-producing capacity of tide-activated goethite and pyrite, microsized highly crystalline pyrite and goethite (>1 μm) were chosen and incubated under redox cycles of microbial reduction and oxidation by oxygen for 1 week. Specifically, 40 mg of pyrite or goethite was added into 36 mL of *Shewanella oneidensis* strain MR-1 solutions (2.5×10^8 cells/mL) containing 20 mM acetate and 50 mM tris-HCl buffer (pH 7.0). The pH of water was set to 7.0, lower than the typical pH of seawater, because coastal water near estuaries is typically mixed with terrestrial fresh water. The solution was incubated anoxically at a higher temperature of 30 °C to enhance microbial activity for 5 days to reach equilibrium. And the incubated temperature was consistent with the field temperature (Table S1). After the preincubation, 4 mL of dipotassium terephthalate (TPA) was injected into the mixture to initiate redox alternating reactions with the final TPA concentration of 1 mM. For the redox cycles of goethite and pyrite, the mixture was oxidized under air for 24 h at 30 °C. Subsequently, the pyrite and goethite suspensions containing *Shewanella oneidensis* strain MR-1 were deoxygenated and incubated under N_2 conditions for another 24 h at 30 °C to complete one redox cycle. The above redox cycle was performed for 7 days. Aliquots (500 μL) were collected and filtrated through a 0.45 μm membrane at selected time points for Fe analyses. After a 7-d incubation, activated iron minerals were washed by ultrapure water and lyophilized for further physicochemical analysis. For the control group at low tide or high tide, the iron suspension was continuously exposed to air or N_2, respectively.

Goethite and Pyrite Characterization. Scanning electron microscopy (SEM) images were taken using a Hitachi SU-8010 microscope equipped with an energy dispersive spectrometer (EDS). High resolution transmission electron microscope (HRTEM) images were taken using a TecnaiG2 microscope after the pyrite was embedded in the epoxy resin and sliced using a microtome. X-ray diffraction (XRD) measurements were performed on a Bruker D8 Advance X-ray diffractometer with Cu Kα radiation (λ = 1.5406 Å) operated at 40 kV and 40 mA.

ROS Quantitation. TPA was used as a chemical probe to quantify hydroxyl radical (•OH) production.[30] Excessive TPA (1 mM) was added to the reaction systems, and •OH production was quantified by determining the product of 2-hydroxyl terephthalate (hTPA) via •OH-mediated hydroxylation of TPA. At designed time points, aliquots (500 μL) were collected from the reaction systems and immediately mixed with methanol (500 μL), followed by filtration through a 0.22 μm membrane to protect the HPLC column. The concentration of hTPA in filtrate was quantified by an Agilent 1260 Infinity II high-performance liquid chromatograph (HPLC) equipped with a fluorescence detector (excitation/emission wavelengths were 250/410 nm). The cumulative concentration of •OH was assessed with a hTPA formation yield of 0.35 upon the hydroxylation of TPA by reacting with

https://doi.org/10.1021/acs.est.3c02302
Environ. Sci. Technol. 2023, 57, 8628−8637

•OH.[6] We note that the yield of hTPA might vary depending on solution conditions, yet it could not affect the major conclusion of this study. The calibration curve of hTPA in seawater and fresh water has no significant difference (Figure S3).

Quantification of Dissolved and Surface Bound Iron. Aliquots (1 mL) were collected at designed intervals from iron mineral suspensions and filtered through a 0.45 μm membrane in an anoxic glovebox (O_2 < 0.1 ppm; Mikrouna, Shanghai Company Ltd., China) to separate dissolved iron from the suspension liquid, followed by the addition of 0.1 mL of HCl (1 M) to the obtained filtrate (0.9 mL) to stabilize iron redox speciation in the solution. Subsequently, the mixture was transferred into a tube containing acetate buffer and 1,10-phenanthroline for dissolved iron analyses.[31] For analysis of ferrous ion adsorbed on the surface of goethite, aliquots (0.9 mL) were sampled at designed intervals and mixed with 0.1 mL of HCl (1 M) for 10 min on a vortex mixer. All adsorbed ferrous ions were assumed to desorb from the solid particles into the acid solution and filtered through a 0.45 μm membrane. Afterward, the filtrate was transferred into a tube containing acetate buffer and 1,10-phenanthroline for total ferrous ion analyses. The characteristic orange-red complex was formed by the reaction of ferrous ion with 1,10-phenanthroline. Surface-bound ferrous ion content was calculated as the difference between total ferrous iron and dissolved ferrous iron.[32]

Electrochemical Analysis. Redox states of pyrite, goethite, and soils were analyzed by electrochemical analysis. All electrochemical measurements were conducted in an anoxic N_2-containing glovebox (O_2 < 0.1 ppm; Mikrouna, Shanghai Company Ltd., China).

Cyclic Voltammetry (CV). CV spectra were collected using a standard three-electrode configuration, with Ag/AgCl/KCl as the reference electrode, a platinum net as the counter electrode, activator-coated glassy carbon as the working electrode, and a 100 mM Na_2SO_4 solution as the electrolyte. The working electrode was prepared by ultrasonicating the iron precipitates (5 mg), acetonitrile (1 mL), and the nafion perfluorinated resin solution (2 μL) for 30 min. The iron mineral suspension (10 μL) was drop-casted onto a glassy carbon electrode. The electrode was then dried at room temperature. The above procedure was repeated three times. CV characterization was conducted on an electrochemical workstation (CHI760E, Chenhua, China).

Mediated Electrochemical Analysis. A 9 mL glassy carbon beaker (Sigradur G, HTW, Germany) served as both the working electrode and the electrochemical reaction vessel. The counter electrode was a platinum wire filled with an electrolyte compartment by a porous glass frit. The reference electrode was Ag/AgCl/KCl. First, the electrolyte buffer (5 mL) with KCl (10 mM) and PBS (10 mM, pH 7) was added into the working electrode and equilibrated to the desired redox potential. Subsequently, 100 μL of stock solutions (10 mM) of zwitterionic viologen 4,4′-bipyridinium-1,1′-bis(2-ethylsulfonate) (ZiV) or 2,2′-azino-bis (3-ethylbenzothiazoline-6-sulfonic acid) (ABTS) as electron transfer mediators were added to the working electrode, resulting in reductive and oxidative current peaks, respectively. After constant background currents were rebalanced, 100 μL samples were injected into the working electrode. The number of electrons transferred to and from postreaction samples were quantified by integration of reductive and oxidative current responses in mediated electrochemical reduction (MER) and oxidation (MEO).

RESULTS AND DISCUSSION

Redox Oscillations Activate Soil Substances for Enhanced ROS Production. We first investigated whether tidal hydrological perturbations-induced redox oscillations could activate soil substances for enhanced ROS production. We chose •OH as a representative ROS species, given it is the most powerful ROS in the environment (standard reduction potential: 2.8 V/SHE[33])[4] and its key roles in accelerating the carbon cycle and other earth surface processes. In addition, •OH is produced through reactions of $O_2^{\bullet-}$ and H_2O_2, and production of •OH also indicates the formation of H_2O_2 and $O_2^{\bullet-}$.[2] We expected that intertidal soils with frequent redox oscillations and supratidal soils with no redox oscillations might exhibit a distinctive different activity for ROS production. The results confirmed our expectations: production of •OH (a highly reactive and biogeochemically important ROS species[34]) in both intertidal and supratidal soils exhibited rhythmic fluctuations under alternating tidal conditions (Figures 1a and S4), while the •OH production in intertidal soils (15.8 ± 0.5 μmol/m^2 at low tide) was 5.9-fold higher than that in supratidal soils (2.7 ± 0.5 μmol/m^2 at low tide).

To verify the impacts of tidal-induced redox oscillations on enhanced ROS-production capability of coastal soils, we incubated the supratidal soils under alternating tidal conditions and examined the activity change. Dissolved oxygen content and redox potential displayed distinct variations with switching between high-tide and low-tide conditions (Figure 1b-c),

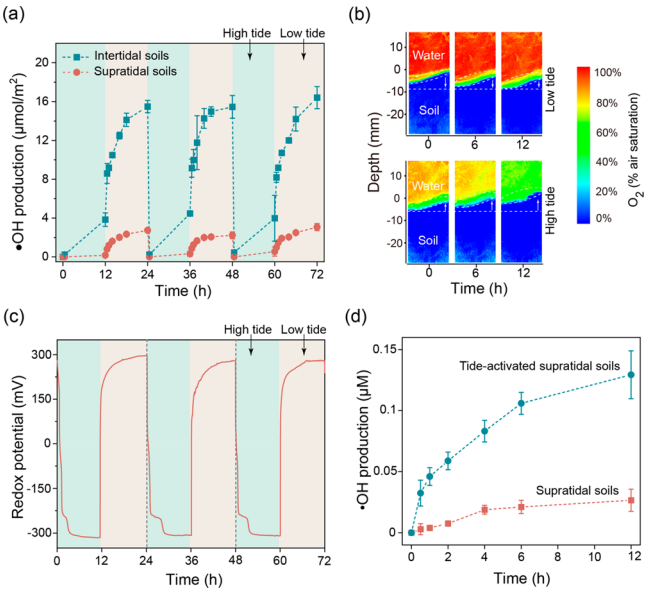

Figure 1. Redox oscillations activate coastal soils for enhanced ROS production. (a) Comparison of ROS production in intertidal and supratidal soils under alternating tidal conditions after normalization because the volume of overlying water was different. After each high tide and low tide cycle, we added new overlying water containing TPA to start the next tidal cycle. The loss of hTPA (e.g., by sorption or radical-mediated processes) was negligible within 24 h.[27] (b-c) Rhythmic oscillations of the oxygen profile and redox potential at the supratidal soil-water interface incubated under alternating tidal conditions. (d) Enhanced ROS production in tide-activated supratidal soils.

https://doi.org/10.1021/acs.est.3c02302
Environ. Sci. Technol. 2023, 57, 8628−8637

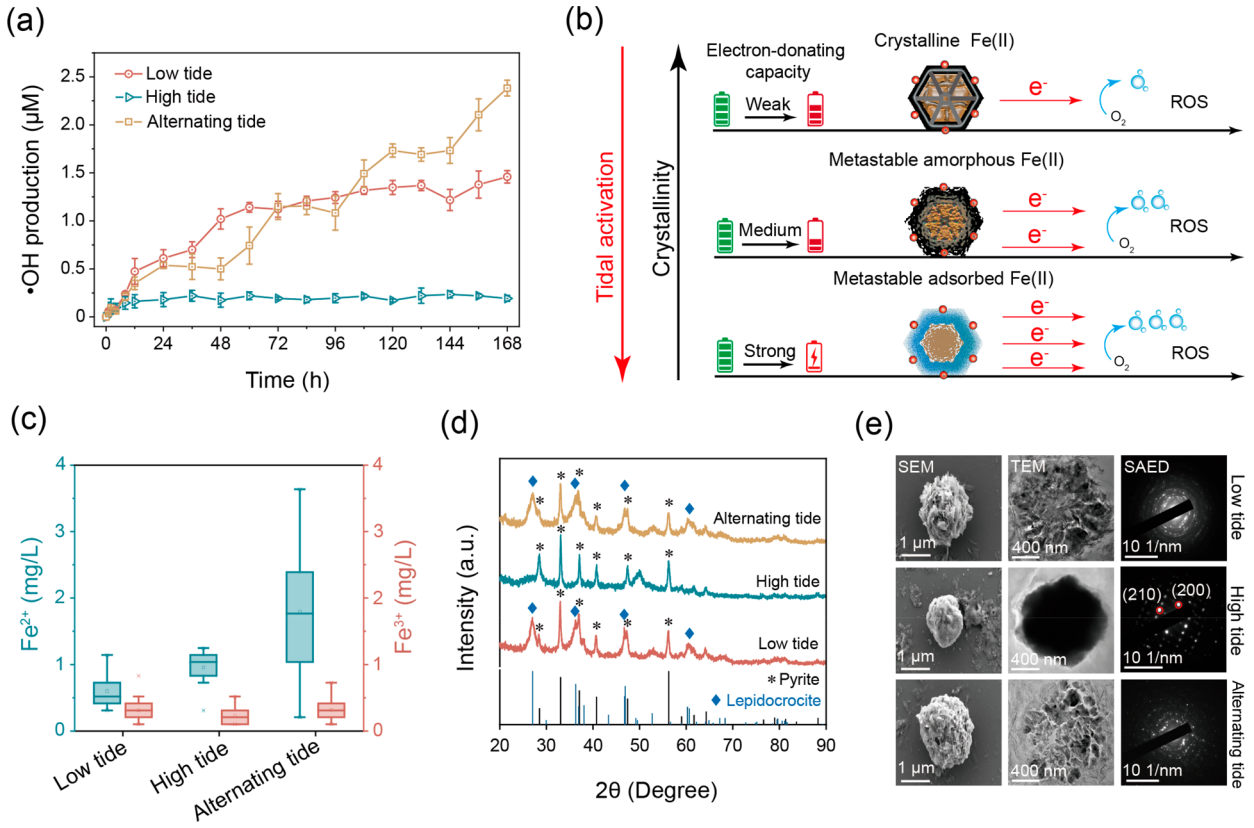

Figure 2. Redox oscillation activation of high-crystalline pyrite for enhanced formation of redox-active metastable phases (RAMPs) and ROS. (a) •OH production by pyrite incubated under high tide, low tide, and alternating tidal conditions. (b) Schematic illustration of the pyrite crystallinity and redox activity variations under tidal activation. (c) Production of Fe^{2+} and Fe^{3+} from pyrite. (d-e) Crystallinity of pyrite under various tidal conditions by X-ray diffraction (XRD) and high-resolution transmission electron microscopy (HRTEM) analyses.

demonstrating the successful buildup of redox oscillations. Microbial respiration depleted dissolved oxygen at the soil-water interface after the rising seawater isolated surface soils from air, leading to the decline in oxygen content at high tide. Upon shifting to low tide, atmospheric oxygen penetrated into the soil, leading to the increase of soil oxygen and redox potential. After a 21-day tidal activation, the •OH production from supratidal soils increased from 0.03 ± 0.01 μM to 0.13 ± 0.02 μM (Figure 1d). This is strong evidence that tide-induced redox oscillations activated soil substances for enhanced ROS production. We preliminarily speculated the frequent redox cycling might induce the transformation of iron minerology in supratidal soils for enhanced ROS production because iron minerals have been identified to be the main contributor for ROS production from soils oxygenation (Figure S5).[4,35,36]

Activation of Reduced Iron Minerals for Enhanced ROS Production. We first examined the production of RAMPs and ROS from reduced iron minerals triggered by tidal hydrology. We chose pyrite, a highly crystalline and reduced iron mineral which is widespread in marine sediments,[34,37] as a representative and environmentally relevant mineral. SEM images showed that pyrite exists as ball-like architecture with diameters of ~1 μm. Energy-dispersive EDS showed that Fe and S were uniformly distributed on pyrite particles (Figure S6). Pyrite appeared highly crystalline, as evidenced by the uniform and ordered diffraction pattern obtained by selected area electron diffraction (SEAD). XRD signals were located at 28.5, 33.0, 37.1, and 59.0 two theta values, corresponding to the (111), (200), (210), and (222) crystal facets,[38] respectively, consistent with the high crystallinity of pyrite (JCPDS No. 99-0087).

Fluctuating redox conditions could enhance ROS production from thermodynamically stable pyrite. Exposure of pyrite at high tide led to negligible •OH production (Figure 2a). At low tide, exposure of pyrite to air resulted in •OH production up to 1.46 ± 0.06 μM. Interestingly, the •OH production from pyrite incubated under alternating tidal conditions was significantly enhanced to 2.4 ± 0.1 μM, suggesting an increased redox activity of pyrite. Pyrite produced less •OH at alternating tide than that at low tide before 96 h because of less oxidation reaction time and insufficient activation of pyrite. The production of •OH by *Shewanella oneidensis* strain MR-1 and sodium acetate without iron minerals was provided in Figure S7. There was no significant change in the production of •OH from *Shewanella oneidensis* strain MR-1 and sodium acetate under anaerobic and aerobic conditions without iron minerals, demonstrating that the ROS production was mainly driven by abiotic Fe-mediated processes. We note that organic matter and bacteria could assist the RAMPs and ROS production by shutting and donating electrons in soils. Production of H_2O_2 from air-exposure of pyrite and the accompanying change in crystallinity of pyrite were given in Figure S8. Hydrogen peroxide could also be generated from pyrite during tidal processes, which accelerated the formation of amorphous metastable iron minerals (e.g., ferrihydrite from the oxidation of pyrite by H_2O_2) from crystalline pyrite. We further incubated the pyrite without *Shewanella oneidensis* strain MR-1 to investigate the role of microorganisms in the

https://doi.org/10.1021/acs.est.3c02302
Environ. Sci. Technol. 2023, 57, 8628−8637

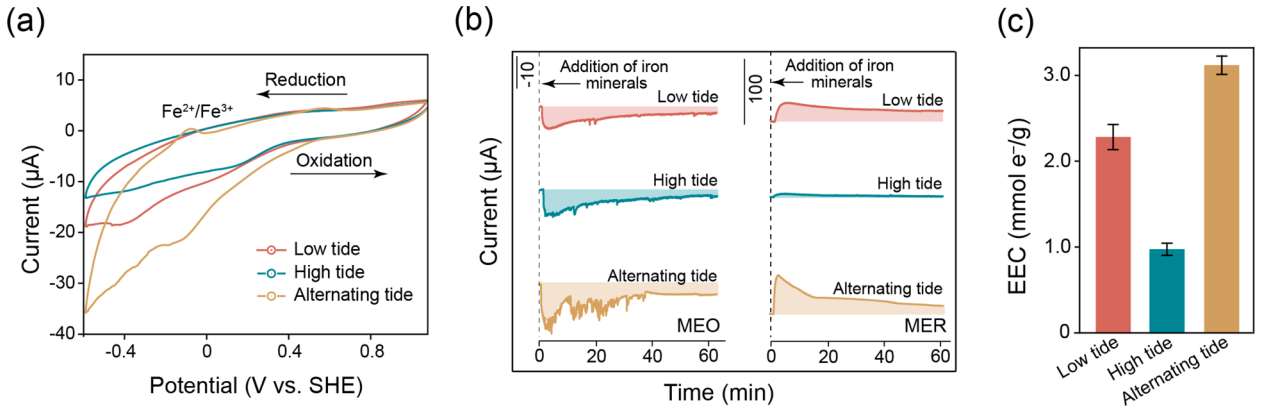

Figure 3. Electrochemical analyses of iron minerals. (a) Current−potential curve (potential was reported versus the standard hydrogen electrode (SHE)), (b) mediated electrochemical oxidation (MEO), mediated electrochemical reduction (MER), and (c) electron exchange capacity (EEC) analyses of pyrite under various tidal conditions.

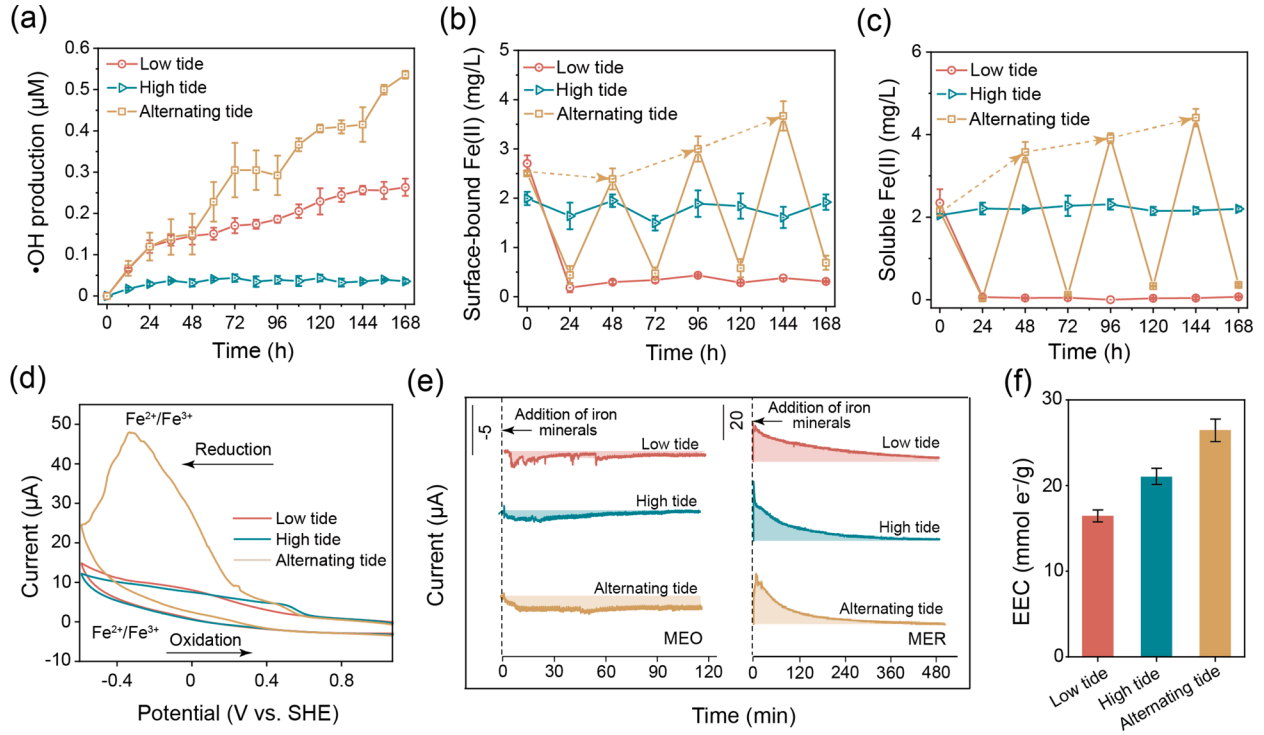

Figure 4. Activation of high-crystalline goethite for enhanced formation of RAMPs and ROS by redox oscillations. (a) Production of •OH by goethite incubated under high tide, low tide, and alternating tidal conditions. (b-c) Production of surface-bound Fe(II) and aqueous Fe(II) from goethite incubated under various tidal conditions. (d-f) Current−potential curve (potential is reported versus the standard hydrogen electrode (SHE)), mediated electrochemical oxidation (MEO), mediated electrochemical reduction (MER), and electron exchange capacity (EEC) analyses of goethite incubated under various tidal conditions.

activation of pyrite. The production of •OH under an alternating tide was much reduced and lower than that of low tide without *Shewanella oneidensis* strain MR-1 (Figure S9), indicating microorganisms played a vital role in increasing the redox activity of pyrite.

Redox oscillations could activate thermodynamically stable pyrite to produce RAMPs. Given that the crystallinity of iron mineral controls the redox activity following the order of adsorbed Fe > amorphous Fe > crystalline Fe,[39] the above results suggest that redox fluctuations likely promote the production of reactive Fe(II) and amorphous Fe on the surface of pyrite.[40] Specifically, the abiotic oxidation of pyrite by air and hydrogen peroxide could produce metastable secondary ferric oxyhydroxides coated on the surface of native pyrite at low tide.[40] Afterward, the amorphous ferric precipitates were readily reduced into dissolved ferrous ions by microbial anaerobic respiration at high tide. The dissolved ferrous ions could be reoxidized into metastable ferric oxyhydroxides precipitates upon shifting to low tide. Iteratively, tide-induced frequent redox cycles of abiotic oxidation and microbial reduction gradually weathered highly crystalline pyrite into RAMPs in coastal surface soils (Figure 2b). Compared to pyrite incubated under low-tide conditions, pyrite incubated under alternating tidal conditions showed a 3.6-fold increase in Fe(II) concentration (Figure 2c). XRD results suggest the formation of RAMPs under tidal fluctuations, with pyrite

https://doi.org/10.1021/acs.est.3c02302
Environ. Sci. Technol. 2023, 57, 8628−8637

crystallinity much decreased coupled to the formation of poorly crystalline lepidocrocite (Figure 2d).[41] HRTEM images showed the least ordered diffraction pattern for pyrite incubated under alternating tidal conditions, further demonstrating its decreased crystalline and the most production of RAMPs (Figures 2e and S10).

The tidal stimulation of the formation of RAMPs was further demonstrated by electrochemical analyses. The current−potential curves show an elevated current for pyrite under alternating tide compared to those obtained under continuous high tide or low tide (Figure 3a).[42] The enhanced pyrite redox activity was further evidenced by the improved currents in MEO and MER after incubation under alternating tide (Figures 3b and S11). While integrating the current over time, the electron exchange capacity (EEC) of pyrite at alternating tide was 3.0 mmol e^-/g, i.e. 1.3- and 3.1-fold higher than those of pyrites at continuous low tide and high tide, respectively (Figure 3c). These results suggest that the tide-induced rapid redox turnover activates the redox-inert crystalline mineral pyrite into redox-active RAMPs that are efficient in mediating electron transfer for ROS production.

Activation of Oxidized Iron Minerals for Enhanced ROS Production. In addition to the reduced iron mineral pyrite, we further examined tide-enhanced production of RAMPs and ROS from an oxidized iron mineral. Goethite (alpha-FeOOH), a ubiquitous and high-crystalline oxidized iron mineral,[43,44] was chosen as an example. Goethite displays a needle-like structure with high crystallinity (Figure S12). Similar to pyrite, negligible $^{\bullet}$OH production was observed for goethite at high tide (Figure 4a). At low tide, exposure of goethite to air resulted in $^{\bullet}$OH production up to 0.25 μM. The slight $^{\bullet}$OH produced by goethite at low tide came from the oxidation of produced Fe(II) during the preincubation. In stark contrast, the $^{\bullet}$OH production from goethite incubated under alternating tidal conditions was significantly enhanced to 0.55 μM. The production of $^{\bullet}$OH from goethite incubated under alternating tidal conditions was much reduced in the absence of *Shewanella oneidensis* strain MR-1 (Figure S13), and there was no Fe(II) generation without *Shewanella oneidensis* strain MR-1, suggesting microbial reduction of goethite was the key to iron mineral activation during tidal alternation (Figure S14). The enhanced $^{\bullet}$OH production is attributed to activation of the high-crystalline goethite into RAMPs by the alternation of anaerobic reduction and aerobic oxidation that exhibit the elevated capability to transfer electrons to oxygen.[45] The RAMPs were mainly formed by dissolved ferrous ions, surface-bound ferrous ions, and amorphous ferric oxyhydroxides derived from goethite. Specifically, microbial anaerobic respiration released electrons to goethite to produce dissolved ferrous ions and surface-bound ferrous ions at high tide.[21,32] Upon shifting to low tide, air penetrated into the mixed-valent iron minerals, leading to the "discharge" of dissolved ferrous ions and surface-bound ferrous ions to oxygen resulting in the formation of amorphous ferric oxyhydroxide precipitates. Recurrently, tide-induced redox oscillations gradually eroded high-crystalline goethite to produce reactive secondary iron minerals that substantially decreased thermodynamic stability of goethite.[45]

Analyses of surface-bound and aqueous Fe(II) confirmed that tidal fluctuations enhanced Fe(II) formation from goethite. The origin ferrous ions produced from goethite during anaerobic preincubation were rapidly oxidized to amorphous ferric oxyhydroxides after exposure to oxygen at low tide. Afterward, the produced secondary ferric oxyhydroxides would be more readily reduced to ferrous ions than crystalline goethite, resulting in progressively increased Fe(II) formation at alternating tide (Figure 4b-c). Further evidence for the tidal activation of goethite came from electrochemical analyses. The current−potential curves showed an increased current peak of iron in goethite after one-week tidal cycles compared to those incubated at continuous high tide or low tide (Figure 4d).[42] The enhanced goethite redox activity was further evidenced by improved currents in MEO and MER after incubation under alternating tides (Figures 4e and S15).[46] The EEC value of goethite under alternating tidal conditions was 25 mmol e^-/g, i.e. 1.5- and 1.2-fold higher than that of goethite at continuous low tide and high tide, respectively (Figure 4f). The above results suggest that both reduced and oxidized redox-inert iron minerals could be activated for enhanced production of RAMPs and ROS under redox oscillations (Figure 5). The disparate capacity to generate RAMPs between pyrite and goethite was primarily attributed to their distinct redox states and corresponding activation requirements.

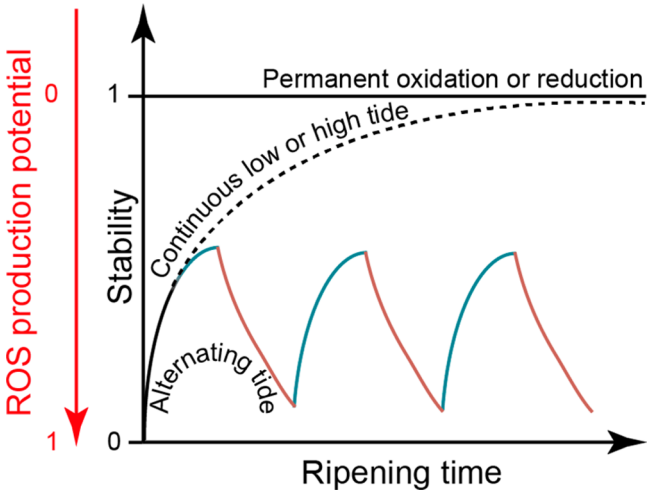

Figure 5. Tidal hydrology interrupted the mineral ripening process and enhanced the formation of RAMPs and ROS from iron minerals.

Tide-Induced Redox Oscillations Ubiquitously Activate Soils for Enhanced ROS Production. We further tested whether tidal fluctuations could ubiquitously activate redox-inert iron-bearing minerals for enhanced ROS production in coastal soils. Coastal soils were collected at six sampling sites along the coast of China (Figure S16). The six sites were chosen based on the varying biogeochemical and climatic conditions[27] and iron minerology properties (Table S2). The diverse coastal soils were redox-deactivated by partially removing the reactive iron through HCl-extraction, leaving highly crystalline iron-bearing minerals in soils that is typically assumed to be less reactive.[47] The $^{\bullet}$OH production from partially deactivated soils obviously decreased compared to that of original soils (showing site 2 as an example). We then reactivated the less reactive crystalline iron-bearing minerals in coastal soils by incubation under alternating tidal conditions for 21 days because partially deactivated soils were more difficult to activate than standard iron minerals. After tidal reactivation, the $^{\bullet}$OH production from all coastal soil samples was dramatically enhanced (1.5−4.9-fold), with cumulative

https://doi.org/10.1021/acs.est.3c02302
Environ. Sci. Technol. 2023, 57, 8628−8637

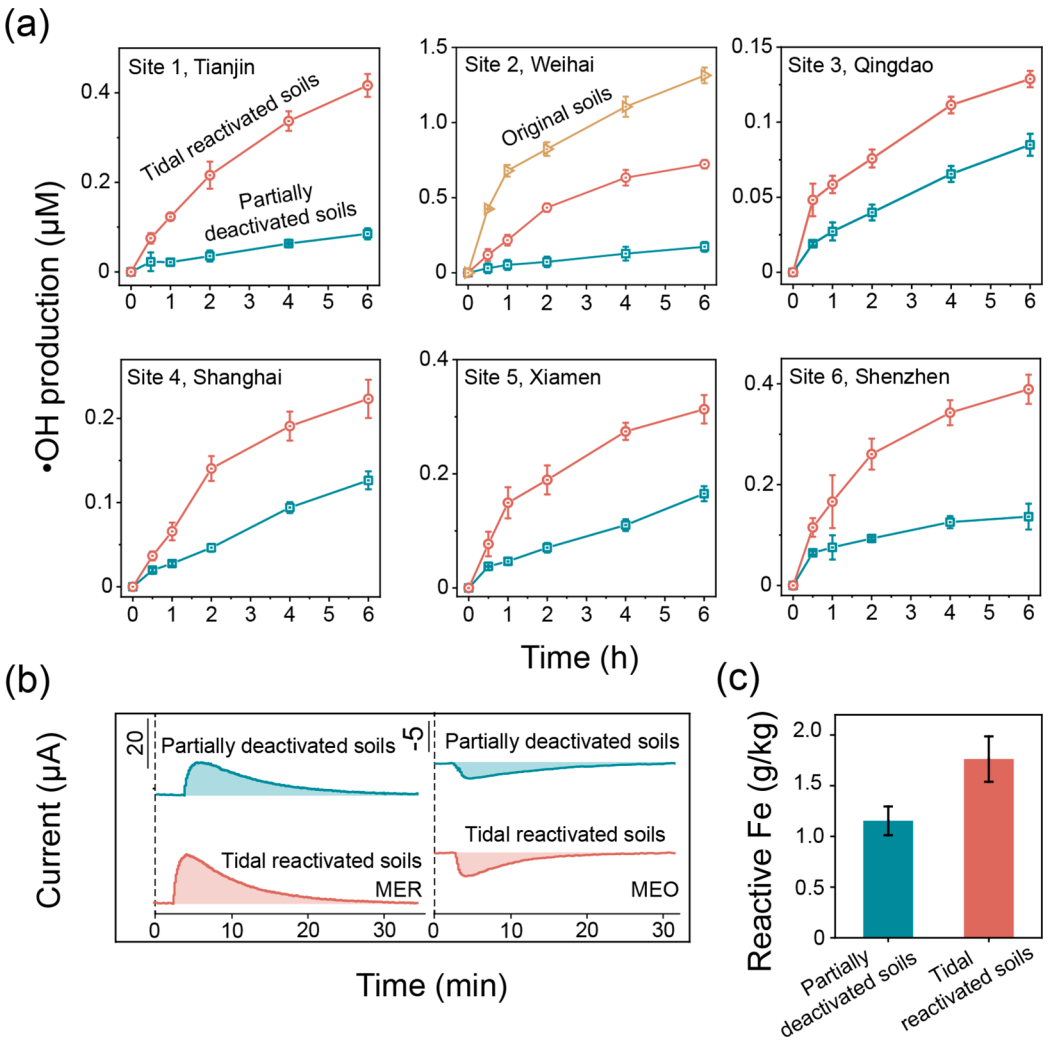

Figure 6. Ubiquitous tidal activation of coastal soils for enhanced production of ROS and RAMPs. (a) Time series of •OH production at sites 1−6 and the enhancement of •OH production in tidal reactivated soils compared to those in partially deactivated soils and original soils (showing site 2 as an example). (b) Mediated electrochemical oxidation (MEO) and mediated electrochemical reduction (MER) of coastal soils (showing site 2 as an example). (c) Reactive iron in coastal soils (showing site 2 as an example). Reactive iron is defined as the fraction of Fe which readily partakes in geochemical reactions in soils or sediments.

•OH over the course of a semidiurnal tide ranging from 0.13 ± 0.01 μM to 0.72 ± 0.03 μM (Figure 6a). The difference in the enhanced amount of •OH production among different sites was mainly due to the diversity in the species and content of iron minerals in soils (Table S2). This enhanced ROS production was linked to improved redox activity of soils, as indicated by higher currents in MEO and MER after tidal incubation (Figure 6b). The tide-induced reactivation of soils was further evidenced by the increased amount of reactive iron derived from the activation of highly crystalline iron in partially deactivated soils (Figure 6c). In addition, the specific surface area of partially deactivated soils increased from 9.3 m^2/g to 17.1 m^2/g after tidal activation, suggesting partial dissolution and reconfiguration of iron minerals in soils probably contributed to the enhanced ROS production (Figure S17). Overall, these results demonstrate that tide-induced redox oscillations could ubiquitously transform and thus activate redox-inert iron minerals into RAMPs coupled with enhanced ROS production capabilities of soils.

■ ENVIRONMENTAL IMPLICATIONS

This study demonstrates that hydrological perturbation-induced redox oscillations can activate both reduced and oxidized high-crystalline iron minerals in soils into RAMPs for enhanced ROS production capability. Notably, the frequency of 1−2 cycles of redox fluctuations per day induced by tidal hydrology is of great importance interrupting the ripening processes and controlling the activation efficiency. In this regard, zones with high frequency redox fluctuations (e.g., intertidal surface soils,[48] rhizosphere soils,[49] hyporheic and riparian soil-water interfaces,[50] surface soils of rain forests[51]) could act as hot spots for RAMP formation that can induce massive ROS production, which can accelerate carbon mineralization and pollutant transformation at these localized soil interfaces where oxygen fluctuates.

Our results also established a link between tidal hydrology and RAMP formation. The enhanced redox activity for activated iron minerals could also induce other biogeochemical processes in addition to enhanced ROS production. For instance, iron mineral-organic matter association is pivotal for carbon persistence in soils and sediments,[52] and iron mineral

https://doi.org/10.1021/acs.est.3c02302
Environ. Sci. Technol. 2023, 57, 8628−8637

activation into RAMPs may promote microbial mineralization of organic carbon through enhanced electron transfer.[53] Moreover, RAMP formation under hydrological perturbations could result in promoted release of combined pollutants (e.g., arsenic)[54,55] and jeopardize soil/groundwater qualities. Finally, we expect that the interfacial electron transfer and structural/chemical changes are key determinants inducing iron mineral activation under fluctuating redox conditions, yet insights into these processes demand development of *in situ* nanoscale imaging techniques, which are being conducted in ongoing work.

■ ASSOCIATED CONTENT

Data Availability Statement

The data that support the findings of this study are available from the corresponding authors upon reasonable request.

Supporting Information

The Supporting Information is available free of charge at https://pubs.acs.org/doi/10.1021/acs.est.3c02302.

Supporting figures, tables, detailed experimental methods, and the results of additional experiments described in the manuscript (PDF)

■ AUTHOR INFORMATION

Corresponding Author

Chiheng Chu − *Department of Environmental Science, Zhejiang University, Hangzhou 310058, China; Zhejiang Provincial Key Laboratory of Organic Pollution Process and Control, Hangzhou 310058, China;* orcid.org/0000-0001-9493-9120; Email: chuchiheng@zju.edu.cn

Authors

Guoqiang Zhao − *Department of Environmental Science, Zhejiang University, Hangzhou 310058, China; Zhejiang Provincial Key Laboratory of Organic Pollution Process and Control, Hangzhou 310058, China;* orcid.org/0000-0002-6632-6412

Mengxi Tan − *Department of Environmental Science, Zhejiang University, Hangzhou 310058, China*

Binbin Wu − *Department of Environmental Science, Zhejiang University, Hangzhou 310058, China*

Xiaoshan Zheng − *Department of Environmental Science, Zhejiang University, Hangzhou 310058, China*

Ruoxuan Xiong − *Department of Environmental Science, Zhejiang University, Hangzhou 310058, China*

Baoliang Chen − *Department of Environmental Science, Zhejiang University, Hangzhou 310058, China; Zhejiang Provincial Key Laboratory of Organic Pollution Process and Control, Hangzhou 310058, China;* orcid.org/0000-0001-8196-081X

Andreas Kappler − *Geomicrobiology, Department of Geoscience, University of Tübingen, Tübingen 72074, Germany; Cluster of Excellence: EXC 2124, Controlling Microbes to Fight Infection, Tübingen 72074, Germany;* orcid.org/0000-0002-3558-9500

Complete contact information is available at: https://pubs.acs.org/10.1021/acs.est.3c02302

Notes

The authors declare no competing financial interest.

■ ACKNOWLEDGMENTS

This work was supported by the National Key Research and Development Program (2022YFC3701400) and the National Natural Science Foundation of China (NSFC, Nos. 22006129, 22136004, 42107392) and Project funded by the China Postdoctoral Science Foundation (CPSF, No. 2022T150565, No. 2021M692774). A.K. acknowledges infrastructural support from the DFG under Germany's Excellence Strategy, Cluster of Excellence EXC2124, project ID 390838134.

■ REFERENCES

(1) Mopper, K.; Zhou, X. Hydroxyl radical photoproduction in the sea and its potential impact on marine processes. *Science* **1990**, *250*, 661−664.

(2) Diaz, J. M.; Hansel, C. M.; Voelker, B. M.; Mendes, C. M.; Andeer, P. F.; Zhang, T. Widespread production of extracellular superoxide by heterotrophic bacteria. *Science* **2013**, *340*, 1223−1226.

(3) Page, S. E.; Kling, G. W.; Sander, M.; Harrold, K. H.; Logan, J. R.; McNeill, K.; Cory, R. M. Dark formation of hydroxyl radical in arctic soil and surface waters. *Environ. Sci. Technol.* **2013**, *47*, 12860−12867.

(4) Tong, M.; Yuan, S.; Ma, S.; Jin, M.; Liu, D.; Cheng, D.; Liu, X.; Gan, Y.; Wang, Y. Production of abundant hydroxyl radicals from oxygenation of subsurface sediments. *Environ. Sci. Technol.* **2016**, *50*, 214−221.

(5) Zhang, T.; Hansel, C. M.; Voelker, B. M.; Lamborg, C. H. Extensive dark biological production of reactive oxygen species in brackish and freshwater ponds. *Environ. Sci. Technol.* **2016**, *50*, 2983−2993.

(6) Chu, C.; Erickson, P. R.; Lundeen, R. A.; Stamatelatos, D.; Alaimo, P. J.; Latch, D. E.; McNeill, K. Photochemical and nonphotochemical transformations of cysteine with dissolved organic matter. *Environ. Sci. Technol.* **2016**, *50*, 6363−6373.

(7) Bonneville, S.; Behrends, T.; Van Cappellen, P. Solubility and dissimilatory reduction kinetics of iron(III) oxyhydroxides: A linear free energy relationship. *Geochimi. Cosmochimi. Ac.* **2009**, *73*, 5273−5282.

(8) Zeng, Q.; Wang, X.; Liu, X.; Huang, L.; Hu, J.; Chu, R.; Tolic, N.; Dong, H. Mutual interactions between reduced fe-bearing clay minerals and humic acids under dark, oxygenated conditions: Hydroxyl radical generation and humic acid transformation. *Environ. Sci. Technol.* **2020**, *54*, 15013−15023.

(9) Chen, N.; Fu, Q.; Wu, T.; Cui, P.; Fang, G.; Liu, C.; Chen, C.; Liu, G.; Wang, W.; Wang, D.; Wang, P.; Zhou, D. Active iron phases regulate the abiotic transformation of organic carbon during redox fluctuation cycles of paddy soil. *Environ. Sci. Technol.* **2021**, *55*, 14281−14293.

(10) Cheng, D.; Neumann, A.; Yuan, S.; Liao, W.; Qian, A. Oxidative degradation of organic contaminants by FeS in the presence of O_2. *Environ. Sci. Technol.* **2020**, *54*, 4091−4101.

(11) Huang, H.; Ji, X.-B.; Cheng, L.-Y.; Zhao, F.-J.; Wang, P. Free radicals produced from the oxidation of ferrous sulfides promote the remobilization of cadmium in paddy soils during drainage. *Environ. Sci. Technol.* **2021**, *55*, 9845−9853.

(12) Peiffer, S.; Kappler, A.; Haderlein, S. B.; Schmidt, C.; Byrne, J. M.; Kleindienst, S.; Vogt, C.; Richnow, H. H.; Obst, M.; Angenent, L. T.; Bryce, C.; McCammon, C.; Planer-Friedrich, B. A biogeochemical-hydrological framework for the role of redox-active compounds in aquatic systems. *Nat. Geosci.* **2021**, *14*, 264−272.

(13) Sheng, A.; Liu, J.; Li, X.; Qafoku, O.; Collins, R. N.; Jones, A. M.; Pearce, C. I.; Wang, C.; Ni, J.; Lu, A.; Rosso, K. M. Labile Fe(III) from sorbed Fe(II) oxidation is the key intermediate in Fe(II)-catalyzed ferrihydrite transformation. *Geochimi. Cosmochimi. Ac.* **2020**, *272*, 105−120.

(14) Aeppli, M.; Kaegi, R.; Kretzschmar, R.; Voegelin, A.; Hofstetter, T. B.; Sander, M. Electrochemical analysis of changes in iron oxide

reducibility during abiotic ferrihydrite transformation into goethite and magnetite. *Environ. Sci. Technol.* **2019**, *53*, 3568−3578.
(15) Kappler, A.; Bryce, C.; Mansor, M.; Lueder, U.; Byrne, J. M.; Swanner, E. D. An evolving view on biogeochemical cycling of iron. *Nat. Rev. Microbiol.* **2021**, *19*, 360−374.
(16) Winkler, P.; Kaiser, K.; Thompson, A.; Kalbitz, K.; Fiedler, S.; Jahn, R. Contrasting evolution of iron phase composition in soils exposed to redox fluctuations. *Geochimi. Cosmochimi. Ac.* **2018**, *235*, 89−102.
(17) Ginn, B.; Meile, C.; Wilmoth, J.; Tang, Y.; Thompson, A. Rapid iron reduction rates are stimulated by high-amplitude redox fluctuations in a tropical forest soil. *Environ. Sci. Technol.* **2017**, *51*, 3250−3259.
(18) Tomaszewski, E. J.; Cronk, S. S.; Gorski, C. A.; Ginder-Vogel, M. The role of dissolved Fe(II) concentration in the mineralogical evolution of Fe (hydr)oxides during redox cycling. *Chem. Geol.* **2016**, *438*, 163−170.
(19) Byrne, J. M.; Klueglein, N.; Pearce, C.; Rosso, K. M.; Appel, E.; Kappler, A. Redox cycling of Fe(II) and Fe(III) in magnetite by Fe-metabolizing bacteria. *Science* **2015**, *347*, 1473−1476.
(20) Bishop, M. E.; Dong, H.; Glasser, P.; Briggs, B. R.; Pentrak, M.; Stucki, J. W.; Boyanov, M. I.; Kemner, K. M.; Kovarik, L. Reactivity of redox cycled Fe-bearing subsurface sediments towards hexavalent chromium reduction. *Geochimi. Cosmochimi. Ac.* **2019**, *252*, 88−106.
(21) Kluepfel, L.; Piepenbrock, A.; Kappler, A.; Sander, M. Humic substances as fully regenerable electron acceptors in recurrently anoxic environments. *Nat. Geosci.* **2014**, *7*, 195−200.
(22) Catallo, W. J. *Hourly and daily variation of sediment redox potential in tidal wetland sediments*; Biological Resources Division Biological Science Report; U.S. Geological Survey: 1999, 1 pp.
(23) Kessler, A. J.; Chen, Y.-J.; Waite, D. W.; Hutchinson, T.; Koh, S.; Popa, M. E.; Beardall, J.; Hugenholtz, P.; Cook, P. L. M.; Greening, C. Bacterial fermentation and respiration processes are uncoupled in anoxic permeable sediments. *Nat. Microbiol.* **2019**, *4*, 1014−1023.
(24) Bertram, C.; Quaas, M.; Reusch, T. B. H.; Vafeidis, A. T.; Wolff, C.; Rickels, W. The blue carbon wealth of nations. *Nat. Clim. Change.* **2021**, *11*, 704−709.
(25) Lv, M.; Luan, X.; Liao, C.; Wang, D.; Liu, D.; Zhang, G.; Jiang, G.; Chen, L. Human impacts on polycyclic aromatic hydrocarbon distribution in Chinese intertidal zones. *Nat. Sustain.* **2020**, *3*, 878−884.
(26) Belliard, J.-P.; Gourgue, O.; Govers, G.; Kirwan, M. L.; Temmerman, S. Coastal wetland adaptability to sea level rise: The neglected role of semi-diurnal vs. diurnal tides. *Limnol. Oceanogr. Lett.* **2023**, *8*, 340−349.
(27) Zhao, G.; Wu, B.; Zheng, X.; Chen, B.; Kappler, A.; Chu, C. Tide-triggered production of reactive oxygen species in coastal soils. *Environ. Sci. Technol.* **2022**, *56*, 11888−11896.
(28) Zhu, C.; van Maren, D. S.; Guo, L.; Lin, J.; He, Q.; Wang, Z. B. Effects of sediment-induced density gradients on the estuarine turbidity maximum in the yangtze estuary. *J. Geophys. Res.: Oceans* **2021**, *126*, e2020JC016927.
(29) Wasmund, K.; Pelikan, C.; Schintlmeister, A.; Wagner, M.; Watzka, M.; Richter, A.; Bhatnagar, S.; Noel, A.; Hubert, C. R. J.; Rattei, T.; Hofmann, T.; Hausmann, B.; Herbold, C. W.; Loy, A. Genomic insights into diverse bacterial taxa that degrade extracellular DNA in marine sediments. *Nat. Microbiol.* **2021**, *6*, 885−898.
(30) Page, S. E.; Arnold, W. A.; McNeill, K. Terephthalate as a probe for photochemically generated hydroxyl radical. *J. Environ. Monitor.* **2010**, *12*, 1658−1665.
(31) Chen, N.; Huang, D.; Liu, G.; Chu, L.; Fang, G.; Zhu, C.; Zhou, D.; Gao, J. Active iron species driven hydroxyl radicals formation in oxygenation of different paddy soils: Implications to polycyclic aromatic hydrocarbons degradation. *Water. Res.* **2021**, *203*, 117484.
(32) Han, R.; Lv, J.; Huang, Z.; Zhang, S.; Zhang, S. Pathway for the production of hydroxyl radicals during the microbially mediated redox transformation of iron (oxyhydr)oxides. *Environ. Sci. Technol.* **2020**, *54*, 902−910.
(33) Zong, Y.; Shao, Y.; Zeng, Y.; Shao, B.; Xu, L.; Zhao, Z.; Liu, W.; Wu, D. Enhanced oxidation of organic contaminants by iron(II)-activated periodate: The significance of high-valent iron−oxo species. *Environ. Sci. Technol.* **2021**, *55*, 7634−7642.
(34) Zhang, P.; Yuan, S. Production of hydroxyl radicals from abiotic oxidation of pyrite by oxygen under circumneutral conditions in the presence of low-molecular-weight organic acids. *Geochim. Cosmochim. Ac.* **2017**, *218*, 153−166.
(35) Xie, W.; Yuan, S.; Tong, M.; Ma, S.; Liao, W.; Zhang, N.; Chen, C. Contaminant degradation by •OH during sediment oxygenation: Dependence on Fe(II) species. *Environ. Sci. Technol.* **2020**, *54*, 2975−2984.
(36) Schaefer, C. E.; Ho, P.; Berns, E.; Werth, C. Mechanisms for abiotic dechlorination of trichloroethene by ferrous minerals under oxic and anoxic conditions in natural sediments. *Environ. Sci. Technol.* **2018**, *52*, 13747−13755.
(37) Gu, X.; Heaney, P. J.; Aarao Reis, F. D. A.; Brantley, S. L. Deep abiotic weathering of pyrite. *Science* **2020**, *370*, eabb8092.
(38) Meng, X.; Li, D.; Chen, L.; He, H.; Wang, Q.; Hong, C.; He, J.; Gao, X.; Yang, Y.; Jiang, B.; Nie, G.; Yan, X.; Gao, L.; Fan, K. High-performance self-cascade pyrite nanozymes for apoptosis−ferroptosis synergistic tumor therapy. *ACS Nano* **2021**, *15*, 5735−5751.
(39) Huang, J.; Jones, A.; Waite, T. D.; Chen, Y.; Huang, X.; Rosso, K. M.; Kappler, A.; Mansor, M.; Tratnyek, P. G.; Zhang, H. Fe(II) redox chemistry in the environment. *Chem. Rev.* **2021**, *121*, 8161−8233.
(40) Zhao, Z.; Peng, S.; Ma, C.; Yu, C.; Wu, D. Redox behavior of secondary solid iron species and the corresponding effects on hydroxyl radical generation during the pyrite oxidation process. *Environ. Sci. Technol.* **2022**, *56*, 12635−12644.
(41) Aromokeye, D. A.; Oni, O. E.; Tebben, J.; Yin, X.; Richter-Heitmann, T.; Wendt, J.; Nimzyk, R.; Littmann, S.; Tienken, D.; Kulkarni, A. C.; Henkel, S.; Hinrichs, K.-U.; Elvert, M.; Harder, T.; Kasten, S.; Friedrich, M. W. Crystalline iron oxides stimulate methanogenic benzoate degradation in marine sediment-derived enrichment cultures. *ISME J.* **2021**, *15*, 965−980.
(42) Yao, J.; Liu, Y.; Zhang, H.; Ma, L.; Meng, T.; Li, N.; Jiang, J.; Zhu, J.; Li, C. M. Configuring optimal FeS2@carbon nanoreactor anodes: Toward insights into pyrite phase change/failure mechanism in rechargeable Ni−Fe cells. *ACS Appl. Mater. Interfaces* **2019**, *11*, 42032−42041.
(43) Seaman, J. C.; Bertsch, P. M.; Strom, R. N. Characterization of colloids mobilized from southeastern coastal plain sediments. *Environ. Sci. Technol.* **1997**, *31*, 2782−2790.
(44) Taylor, S. D.; Liu, J.; Zhang, X.; Arey, B. W.; Kovarik, L.; Schreiber, D. K.; Perea, D. E.; Rosso, K. M. Visualizing the iron atom exchange front in the Fe(II)-catalyzed recrystallization of goethite by atom probe tomography. *P. NATL. ACAD. SCI. USA* **2019**, *116*, 2866−2874.
(45) Orsetti, S.; Laskov, C.; Haderlein, S. B. Electron transfer between iron minerals and quinones: Estimating the reduction potential of the Fe(II)-goethite surface from AQDS speciation. *Environ. Sci. Technol.* **2013**, *47*, 14161−14168.
(46) Klüpfel, L.; Keiluweit, M.; Kleber, M.; Sander, M. Redox properties of plant biomass-derived black carbon (biochar). *Environ. Sci. Technol.* **2014**, *48*, 5601−5611.
(47) Wallmann, K.; Hennies, K.; Konig, I.; Petersen, W.; Knauth, H. D. New procedure for determining reactive Fe(III) and Fe(II) minerals in sediments. *Limnol. Oceanogr.* **1993**, *38*, 1803−1812.
(48) LaRiviere, D.; Autenrieth, R. L.; Bonner, J. S. Redox dynamics of a tidally-influenced wetland on the San Jacinto River. *Estuaries* **2004**, *27*, 253−264.
(49) Dai, H.; Wu, B.; Chen, B.; Ma, B.; Chu, C. Diel fluctuation of extracellular reactive oxygen species production in the rhizosphere of rice. *Environ. Sci. Technol.* **2022**, *56*, 9075−9082.
(50) Zhang, N.; Bu, X.; Li, Y.; Zhang, Y.; Yuan, S.; Wen, Z.; Tong, M.; Lin, L. Water table fluctuations regulate hydrogen peroxide

production and distribution in unconfined aquifers. *Environ. Sci. Technol.* **2020**, *54*, 4942−4951.
(51) Bhattacharyya, A.; Campbell, A. N.; Tfaily, M. M.; Lin, Y.; Kukkadapu, R. K.; Silver, W. L.; Nico, P. S.; Pett-Ridge, J. Redox fluctuations control the coupled cycling of iron and carbon in tropical forest soils. *Environ. Sci. Technol.* **2018**, *52*, 14129−14139.
(52) Kleber, M.; Bourg, I. C.; Coward, E. K.; Hansel, C. M.; Myneni, S. C. B.; Nunan, N. Dynamic interactions at the mineral−organic matter interface. *Nat. Rev. Earth. Env.* **2021**, *2*, 402−421.
(53) Chen, C.; Hall, S. J.; Coward, E.; Thompson, A. Iron-mediated organic matter decomposition in humid soils can counteract protection. *Nat. Commun.* **2020**, *11*, 2255.
(54) Stolze, L.; Battistel, M.; Rolle, M. Oxidative dissolution of arsenic-bearing sulfide minerals in groundwater: Impact of hydrochemical and hydrodynamic conditions on arsenic release and surface evolution. *Environ. Sci. Technol.* **2022**, *56*, 5049−5061.
(55) Connolly, C. T.; Stahl, M. O.; DeYoung, B. A.; Bostick, B. C. Surface flooding as a key driver of groundwater arsenic contamination in southeast asia. *Environ. Sci. Technol.* **2022**, *56*, 928−937.

https://doi.org/10.1021/acs.est.3c02302
Environ. Sci. Technol. 2023, 57, 8628−8637